International Journal of Heat and Mass Transfer 54 (2011) 4988–5000

Contents lists available at ScienceDirect

International Journal of Heat and Mass Transfer

journal homepage: www.elsevier.com/locate/ijhmt

Saturated flow boiling heat transfer of R-410A and associated bubble characteristics in a narrow annular duct

C.A. Chen, K.W. Li, Y.M. Lie, T.F. Lin *

Department of Mechanical Engineering, National Chiao Tung University, Hsinchu, 1001 Ta Hsueh Road, Hsinchu 30010, Taiwan, ROC

ARTICLE INFO

Article history:
Received 10 October 2010
Received in revised form 7 May 2011
Accepted 7 May 2011
Available online 30 July 2011

Keywords:
Saturated flow boiling heat transfer
R-410A
Bubble characteristics
Mini-channel

ABSTRACT

Experiments are conducted here to investigate how the channel size affects the R-410A saturated flow boiling heat transfer and associated bubble characteristics in a horizontal narrow annular duct. The gap of the duct is fixed at 1.0 and 2.0 mm in this study. The measured data indicate that the saturated flow boiling heat transfer coefficient increases with increasing refrigerant mass flux and saturated temperature and with a decrease in the gap size. Besides, raising the imposed heat flux can cause a significant increase in the boiling heat transfer coefficient. The results from the flow visualization show that the mean diameter of the bubbles departing from the heating surface decreases slightly with increasing refrigerant mass flux and saturated temperature. Moreover, the bubble departure frequency increases at reducing duct size and increasing mass flux. And at a high imposed heat flux many bubbles generated from the cavities in the heating surface tend to merge together to form big bubbles. Meanwhile, comparisons of the present heat transfer data for R-410A with R-407C and R-134a in the same duct and with some existing correlations are conducted. Furthermore, an empirical correlation for the present R-410A saturated flow boiling heat transfer data is proposed.

1. Introduction

Choosing a suitable refrigerant plays an important part in the design of air conditioning and refrigeration systems. In addition, the chlorofluorocarbons refrigerants (CFCs) have been completely prohibited in production since 1996 and the hydrochlorofluorocarbons refrigerants (HCFCs) will be phased out by 2020, due to the presence of chlorine and carbon in these refrigerants which are depleting the earth's stratospheric ozone layer and increasing the Total Equivalent Warming Impact (TEWI). Thus, the substitution of CFCs and HCFCs becomes urgent recently. The hydrofluorocarbons refrigerants (HFCs) such as R-134a, R-407C, R-410A, R-410B and R-507 are considered to be the eligible alternatives and some are currently in use.

The literature relevant to the present study is reviewed in the following. In air conditioning and refrigeration systems, small channel with its small volume, lower total mass and low inventory of working fluid is a favorable option for compact heat exchangers to improve the boiling and condensation heat transfer performance. It is important to comprehend the boiling and condensation heat transfer and flow characteristics in the small channels consisted in compact heat exchangers. The channel size in a compact heat exchanger can significantly affect the performance of the exchanger [1]. In sizing the small channels, Kandlikar and Grande [2] proposed that for the conventional channels $D_h > 3$ mm, for the mini-channels 200 μm < D_h < 3 mm, and for the micro-channels 10 μm < D_h < 200 μm. On the contrary, Kew and Cornwell [3] introduced the Confinement number, $N_{conf} = \frac{(\sigma/(g\Delta\rho))^{0.5}}{D_h}$, which represents the importance of the flow restriction by the small size channel. They showed that the effects of the channel size became extremely substantial when $N_{conf} > 0.5$.

Flow boiling of refrigerants R-11 and R-123 in a horizontal small copper tube (D_h = 1.95 mm) investigated by Bao et al. [4] showed that the heat transfer coefficients were independent of the refrigerant mass flux and vapor quality, but were a strong function of the wall heat flux. Nucleate boiling was noted to be the dominant mechanism over a wide range of the tested flow conditions. Tran et al. [5] examined flow boiling of refrigerant R-12 in small circular and rectangular channels (D_h = 2.46 and 2.4 mm). Two distinct two-phase flow regions were noted, the convective boiling dominant region at lower wall superheat (<2.75 K) and nucleate boiling dominant region at higher wall superheat (>2.75 K). The differences in the boiling heat transfer coefficients in the circular and rectangular tubes are small. The R-134a experimental data taken from an upward vertical rectangular multichannel (D_h = 2.01 mm) by Agostini and Bontemps [6] concluded that bubble nucleation was the dominant mechanism for the heat flux higher than 14 kW/m^2 and wall superheat higher than 3 K, and the transition from the boiling dominated by bubble nucleation to

* Corresponding author.
E-mail address: tflin@mail.nctu.edu.tw (T.F. Lin).

0017-9310/$ - see front matter © 2011 Elsevier Ltd. All rights reserved.
doi:10.1016/j.ijheatmasstransfer.2011.07.012

Nomenclature

A_s	outside surface area of the heated inner pipe (m^2)
Bo	Boiling number, $Bo = \frac{q}{G \cdot i_{fg}}$, dimensionless
c_p	specific heat (J/kg °C)
D_i, D_o	inner and outside diameters of duct (m)
D_h	hydraulic diameter (m), $D_h = (D_o - D_i)$
D_p	dimensionless mean bubble departure diameter
d_p	bubble departure diameter (m)
F_d	dimensionless mean bubble departure frequency
f	bubble departure frequency
f_f	friction factor
g	acceleration due to gravity (m/s^2)
G	mass flux (kg/m^2 s)
h_r	boiling heat transfer coefficient (W/m^2 °C)
i_{fg}	enthalpy of vaporization (J/kg)
k_l	liquid thermal conductivity (W/m °C)
n_{ac}	active nucleation site density (n/m^2)
N_{AC}	dimensionless active nucleation site density
N_{conf}	Confinement number, $N_{conf} = \frac{(\sigma/(g\Delta\rho))^{0.5}}{D_h}$, dimensionless
Nu	Nusselt number, $Nu = \frac{hD_h}{k}$, dimensionless
P	system pressure (kPa)
Pr	Prandtl number, $Pr = \frac{\mu \cdot c_p}{k}$, dimensionless
q	average imposed heat flux (W/m^2)
q_b, q_c, q_t	heat flux due to bubble nucleation, single-phase convection, total value (W/m^2)
Q_n	net power input (W)
Re_l	Reynolds number of liquid in two-phase flow, $Re_l = \frac{GD_h(1-x)}{\mu_l}$, dimensionless
T_w	wall temperature of heated inner pipe (°C)
T_{sat}	saturated temperature of the refrigerant (°C)
x	vapor quality
z	downstream coordinate for annular duct flow measured from duct inlet (mm)

Greek symbols

ΔT_{sat}	wall superheat, $(T_w - T_{sat})$ (°C)
δ	gap size of duct (mm)
μ_l	viscosity of liquid R-410A (N s/m^2)
ρ_g, ρ_l	vapor and liquid densities (kg/m^3)
$\Delta\rho$	density difference, $\Delta\rho = \rho_l - \rho_g$ (kg/m^3)
σ	surface tension (N/m)

convection occurred at $Bo \cdot (1 - x) \approx 2.2 \times 10^{-4}$. Kandlikar and Steinke [7] found that for a refrigerant with a high liquid-to-vapor density ratio, the convective effects dominated as the vapor quality increased. This led to an increasing trend in the boiling heat transfer coefficient at increasing vapor quality. A high boiling number results in a higher nucleate boiling contribution, which tends to decrease as the vapor quality increases, causing a decreasing trend in heat transfer coefficient with increasing vapor quality. An experimental study for the flow boiling of refrigerant R-141b in a vertical tube (D_h = 1 mm) conducted by Lin et al. [8] concluded that at low vapor quality nucleate boiling dominated. But at higher vapor quality convective boiling dominates. In a review article Watel [9] concluded that convective boiling dominated at low heat fluxes and wall superheats and high vapor qualities, otherwise nucleate boiling dominated.

Flow boiling of refrigerant R-410A in conventional smooth and finned tubes was investigated respectively by Wang et al. [10] and Ebisu and Torikoshi [11] and by Hsieh et al. [12]. They noted that the boiling heat transfer coefficients of R-410A were higher than refrigerant R-22 except at high vapor qualities and the coefficients increase with the imposed heat flux and mass flux. Similar trends were found by Hsieh and Lin [13,14] and by Longo and Gasparella [15] and Kim et al. [16] for boiling of R-410A in plate heat exchanges.

The effects of lubricant oils on the two-phase heat transfer characteristics are important in designing vapor compression air-conditioning and refrigeration systems and have been the subject of many studies. Detailed reviews on the subject are available from Schlager et al. [17,18] and Gidwani et al. [19]. Lottin et al. [20] examined the effects of synthetic lubricants on a refrigeration system using R-410A. They concluded that the influences of the oils on the system performance were negligible when the oils did not exceed 0.5% of the total refrigerant weight. Beyond this value the performance decreases substantially.

To elucidate the flow boiling heat transfer mechanisms in small channels, we need to delineate the prevailing two-phase flow regimes. Cornwell and Kew [21] explored possible flow regimes for boiling of refrigerant R-113 in a vertical rectangular multi-channel with D_h = 1.03 and 1.64 mm. Based on visualization of the boiling flow and measurement of the heat transfer, three flow regimes have been identified, namely, the isolated bubble, confined bubble and annular-slug bubble flows. In the isolated bubble regime, the heat transfer coefficient depends on the heat flux and hydraulic diameter. In the confined bubble regime, the heat transfer coefficient depends on the mass flux and vapor quality. While in the annular-slug bubble regime, heat transfer coefficient is a function of the mass flux, vapor quality and hydraulic diameter.

It has been known for some time that bubble characteristics such as bubble departure frequency, growth, sliding and departure size play an important role in flow boiling heat transfer. Yin et al. [22] examined some bubble characteristics associated with subcooled flow boiling of refrigerant R-134a in a horizontal annular duct (D_h = 10.31 mm). They noted that the bubble departure frequency was suppressed by raising the mass flux and subcooling of R-134a, and only the liquid subcooling significantly affected the bubble departure size. Visualization of subcooled flow boiling of upward water flow in a vertical annular channel (D_h = 19 mm) by Situ et al. [23] suggested that generally the bubble departure frequency increased with the heat flux and the bubble growth rate dropped sharply after the bubble lift-off. The study of water boiling in a horizontal rectangular channel with one side heated (D_h = 40 mm) conducted by Maurus et al. [24] manifested that the waiting time between two bubble cycles decreased significantly at increasing mass flux. Chang et al. [25] studied the near-wall bubble behavior for water boiling in a vertical one-side heated rectangular channel (D_h = 4.44 mm). They showed that the size of coalesced bubbles decreased for an increase in the water mass flux and the mass flux only exhibits a strong effect on the bubble size. Del Balle and Kenning [26] examined the subcooled flow boiling for water in a rectangular vertical channel and found that the maximum bubble diameter was independent of the heat flux. An experimental study on the bubble rise path after its departure from a nucleation site for water in a vertically upward tube (D_h = 20 mm) by Okawa et al. [27] suggested that the inertia force significantly influenced the onset of bubble detachment and the shear force induced a lift force to detach the bubble from the wall.

An early general empirical correlation model for flow boiling in channels was proposed by Chen [28]. He divided the boiling heat transfer coefficient into two parts: a microconvective (nucleate boiling) contribution estimated by the pool boiling correlations and a macroconvective (non-boiling forced convection) contribution estimated by the single-phase correlation such as the

Dittus–Boelter equation [29]. In order to account for the diminished contribution of nucleate boiling as the forced convective effects increased at a higher vapor quality, he introduced an enhancement factor E and a suppression factor S to respectively accommodate the forced convection augmentation and nucleate boiling retardation. Gungor and Winterton [30] modified Chen's correlation and proposed correlations for the enhancement and suppression factors. An improved correlation from Liu and Winterton [31] introduced an asymptotic function to predict boiling heat transfer coefficient for vertical and horizontal flows in tubes and annuli. Later Zhang et al. [32] modified Chen's correlation to predict the heat transfer in mini channels. Besides, Tran et al. [5] modified the heat transfer correlation of Lazarek and Black [33] with the Reynolds number of the flow replaced by the Weber number to eliminate viscous effects in favor of the influences from the surface tension. Similar correlations were proposed by Fujita et al. [34].

Kandlikar [35] proposed a general correlation for saturated flow boiling heat transfer in horizontal and vertical tubes. The correlation is also based on a model similar to that of Chen [28]. In a following study [36,37], he developed correlations to predict transition, laminar and deep laminar flows in mini-channels and micro-channels. A new correlation for boiling heat transfer in small diameter channels was proposed by Cornwell and Kew [21]. The correlation was divided by the three two-phase flow regimes based on the value of the Confinement number.

The above literature review clearly indicates that flow boiling heat transfer of HFC refrigerants in small diameter channels remains largely unexplored. In the recent studies [38–41] we report experimental data for the saturated and subcooled flow boiling heat transfer of refrigerants R-134a and R-407C and associated bubble characteristics in a horizontal narrow annular duct. In the present study we move further to investigate the R-410A saturated flow boiling in the same duct. Data from this study for R-410A will be compared with those for R-134a and R-407C reported in the previous studies [38,40] and with some existing correlations for small diameter channels proposed in the open literature.

2. Experimental apparatus and procedures

The experimental system modified slightly from that used in the previous study [38] is employed here to investigate the saturated flow boiling heat transfer of R-410A in a narrow annular duct. It is schematically depicted in Fig. 1. The experimental apparatus consists of three main loops, namely, a refrigerant loop, a water-glycol loop, and a hot-water loop. Refrigerant R-410A is circulated in the refrigerant loop. In order to control various test conditions of the refrigerant in the test section, we need to control the temperature and flow rate in the other two loops.

As schematically shown in Fig. 2, the test section of the experimental apparatus is a horizontal annular duct with the outer pipe made of Pyrex glass to permit the visualization of boiling processes in the refrigerant flow. The glass pipe is 160-mm long with an inside diameter of 20.0 mm. Its wall is 4.0-mm thick. Both ends of the pipe are connected with copper tubes of the same size by means of flanges and are sealed by O-rings. The inner copper pipe has 16.0 or 18.0-mm nominal outside diameter with its wall being 1.5 or 2.5-mm thick and is 0.41-m long. Thus the gap of the annular duct is 2.0 or 1.0 mm (D_h = 4.0 or 2.0 mm). Note that the heated surface characteristics are important in the bubble nucleation and subsequent growth processes. To reduce the surface roughness, the outside surface of the inner pipe is polished successively by fine sandpapers of No. 1000, 2000, 3000 and then cleaned by ethanol. Besides, to insure the gap between the inner and outer pipes being uniform, we first measure the outside diameter of the inner pipe and the inside diameter of the glass pipe by digital calipers whose resolutions are 0.001 mm with the measurement accuracy of ±0.01 mm. Then we photo the top and side view pictures of the annular duct and measure the average radial distance from the inside surface of the glass pipe to the outside surface of the inner tube. From the above procedures the duct gap is ascertained and its uncertainty is estimated to be 0.02 mm. It is also noted that the flow enters the duct long before the heated section with the entry length of 93 mm so that the entrance effects on the boiling are small. An electric cartridge heater of 160 mm in length and 12.5 mm in diameter with a maximum power output of 800 W is inserted into the inner pipe. Furthermore, the pipe has an inactive heating zone of 10-mm long at each end and is insulated with Teflon blocks and thermally nonconducting epoxy to minimize heat loss from it. Thermal contact between the heater and the inner pipe is improved by coating a thin layer of heat-sink compound on the heater surface before installing the heater. Then, 8 T-type calibrated thermocouples are electrically insulated by electrically nonconducting thermal bond before they are fixed on the inside surface of the inner pipe so that the voltage signals from the thermocouples are not interfered with the DC current passing through the cartridge heater. The thermocouples are positioned at three axial stations along the inner pipe. At each axial station, two to four thermocouples are placed at top, bottom, or two sides of the pipe circumference with 180° or 90° apart. The outside surface temperature of the inner pipe T_w is then derived from the measured inside surface temperature by taking the radial heat conduction through the pipe wall into account.

The photographic apparatus established in the present study to record the bubble characteristics in the saturated flow boiling of R-410A in the annular duct consists of an IDT X-Stream™ VISION XS-4 high speed CMOS digital camera, a Mitutoyo micro lens set, a 3D positioning mechanism, and a personal computer. The high-speed digital camera can take photographs up to 143,307 frames/s with an image resolution of 512×16. Here, a recording rate of 10,000 frames/s with the highest image resolution of 512×256 is adopted to obtain the images of the bubble ebullition processes in the boiling flow. The data for some bubble characteristics are collected in the regions around the middle axial location (z = 80 mm). After the experimental system reaches a statistically steady state, we start recording the boiling activity. The high-speed digital camera can store the images which are later downloaded to the personal computer. Then, the mean bubble departure diameter and frequency and mean active nucleation site density are calculated by viewing more than 1000 frames at z = 80 mm.

Before a test is started, the temperature of refrigerant R-410A in the test section is compared with its saturation temperature corresponding to the measured saturation pressure and the allowable difference is kept in the range of 0.2–0.3 K. Otherwise, the system is re-evacuated and then re-charged to remove the air existing in the refrigerant loop. A vacuum pump is used to evacuate noncondensable gases in the system to a low pressure of 0.067 Pa in the loop. In the test the liquid refrigerant at the inlet of the test section is first maintained at the saturated state by adjusting the water-glycol temperature and flow rate. In addition, we adjust the thermostat temperature in the water loop to stabilize the refrigerant temperature at the test section inlet. Then, we regulate the refrigerant pressure at the test section inlet by adjusting the opening of the gate valve locating right after the exit of the test section. Meanwhile, by changing the current of the DC motor connecting to the refrigerant pump, the refrigerant flow rate can be varied. The imposed heat flux from the heater to the refrigerant is adjusted by varying the electric current delivered from the DC power supply. By measuring the current delivered to and voltage drop across the heater and by photographing the bubble activity, we can calculate the heat transfer rate to the refrigerant and obtain the bubble

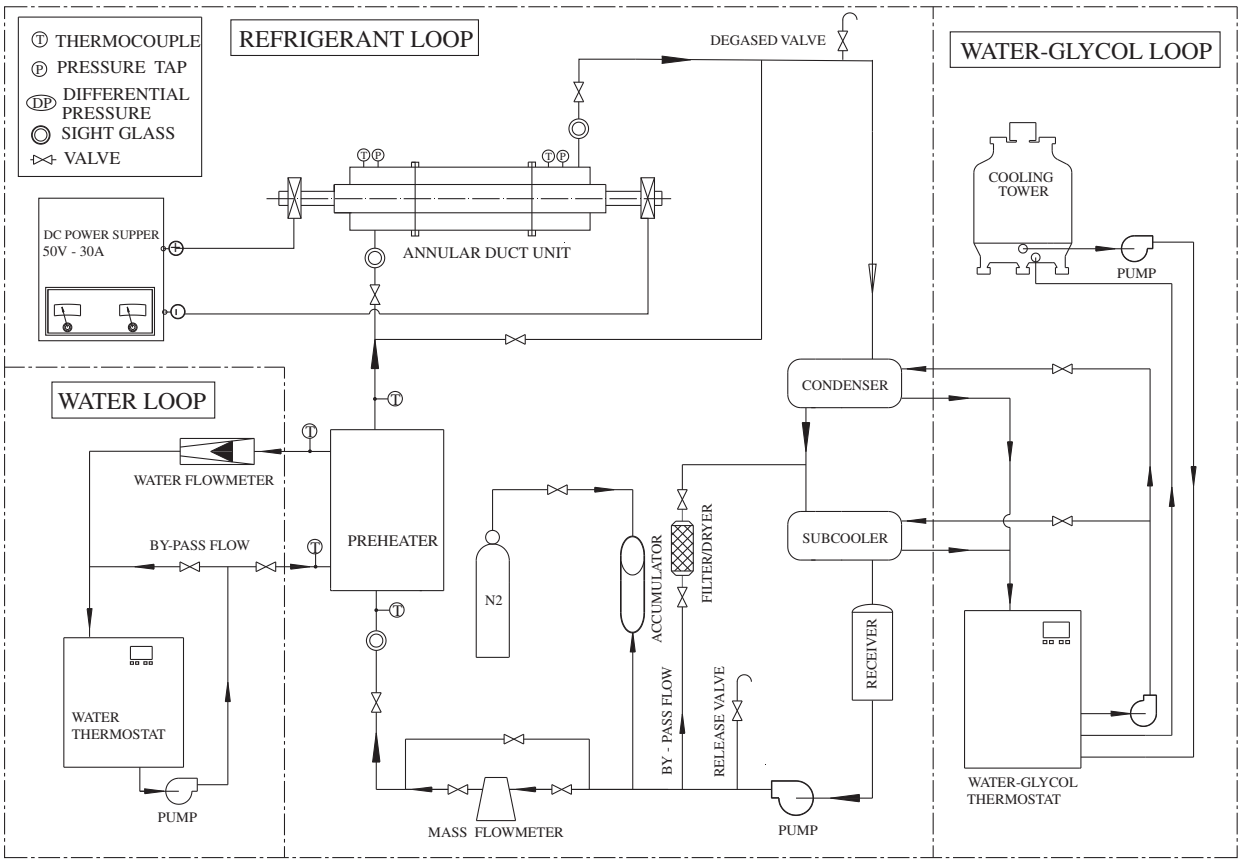

Fig. 1. Schematic of experimental system for the annular duct.

characteristics. All tests are run at statistically steady-state conditions. The whole system is considered to be at a statistically steady state when the time variations of the system pressure and imposed heat flux are respectively within ±1% and ±4%, and the time variations of the heated wall temperature are less than ±0.2 °C for a period of 100 min. Then all the data channels are scanned every 0.5 s for a period of 20 s. The data repeatability is insured by measuring each data point three times and the deviations of the measured values from their averages should be all less than 5%.

3. Data reduction and verification of experimental system

The imposed heat flux q to the refrigerant flow in the annular duct is calculated on the basis of the net power input Q_n and the total outside surface area of the inner pipe of the annular duct A_s as $q = Q_n/A_s$. The total power input Q_t is obtained from the product of the measured voltage drop across the cartridge heater and electric current passing through it. Hence the net power input to the test section is equal to $(Q_t - Q_{loss})$.

The total heat loss from the test section Q_{loss} is evaluated from the correlation for natural convection around a circular cylinder by Churchill and Chu [42]. To reduce the heat loss from the test section, it is covered with a polyethylene insulation layer. The results from this heat loss test indicate that the total heat loss from the test section is generally less than 1% of the total power input no matter when single-phase flow or two-phase boiling flow is in the duct. The saturated flow boiling heat transfer coefficient at a given axial location is defined as

$$h_r = \frac{Q_n/A_s}{(T_w - T_{sat})} \tag{1}$$

Uncertainties of the measured heat transfer coefficients are estimated according to the procedures proposed by Kline and McClintock [43] for the propagation of errors in physical measurement. The results from this uncertainty analysis are summarized in Table 1.

In order to check the suitability of the experimental system for measuring the flow boiling heat transfer coefficients, the single-phase liquid R-410A heat transfer data for the liquid Reynolds number ranging from 4487 to 18,844 are measured first and compared with the well-known traditional forced convection correlation proposed by Gnielinski [44], as that in the previous studies [38–41]. The results manifest that the present data can be well correlated by his correlation with a mean absolute error of 4.8%. Thus the established system is considered to be suitable for the present R-410A flow boiling experiment.

4. Results and discussion

The present R-410A flow boiling experiments are performed for the refrigerant mass flux G varying from 300 to 700 kg/m^2 s, imposed heat flux q ranging from 0 to 45 kW/m^2, and system pressure P set at 1100 kPa and 1250 kPa (corresponding to the R-410A saturation temperature T_{sat} = 10 °C and 15 °C) for the gap of the duct δ = 1.0 and 2.0 mm. The ranges of the parameters chosen above are in accordance with some air-conditioning applications. The measured boiling heat transfer data expressed in terms of the boiling curves and boiling heat transfer coefficient are examined first. Then, selected flow photos and data deduced from the images of the boiling processes taken at a small region around the middle axial station z = 80 mm are presented to illustrate the bubble characteristics in the boiling flow. Besides, comparisons with the data for

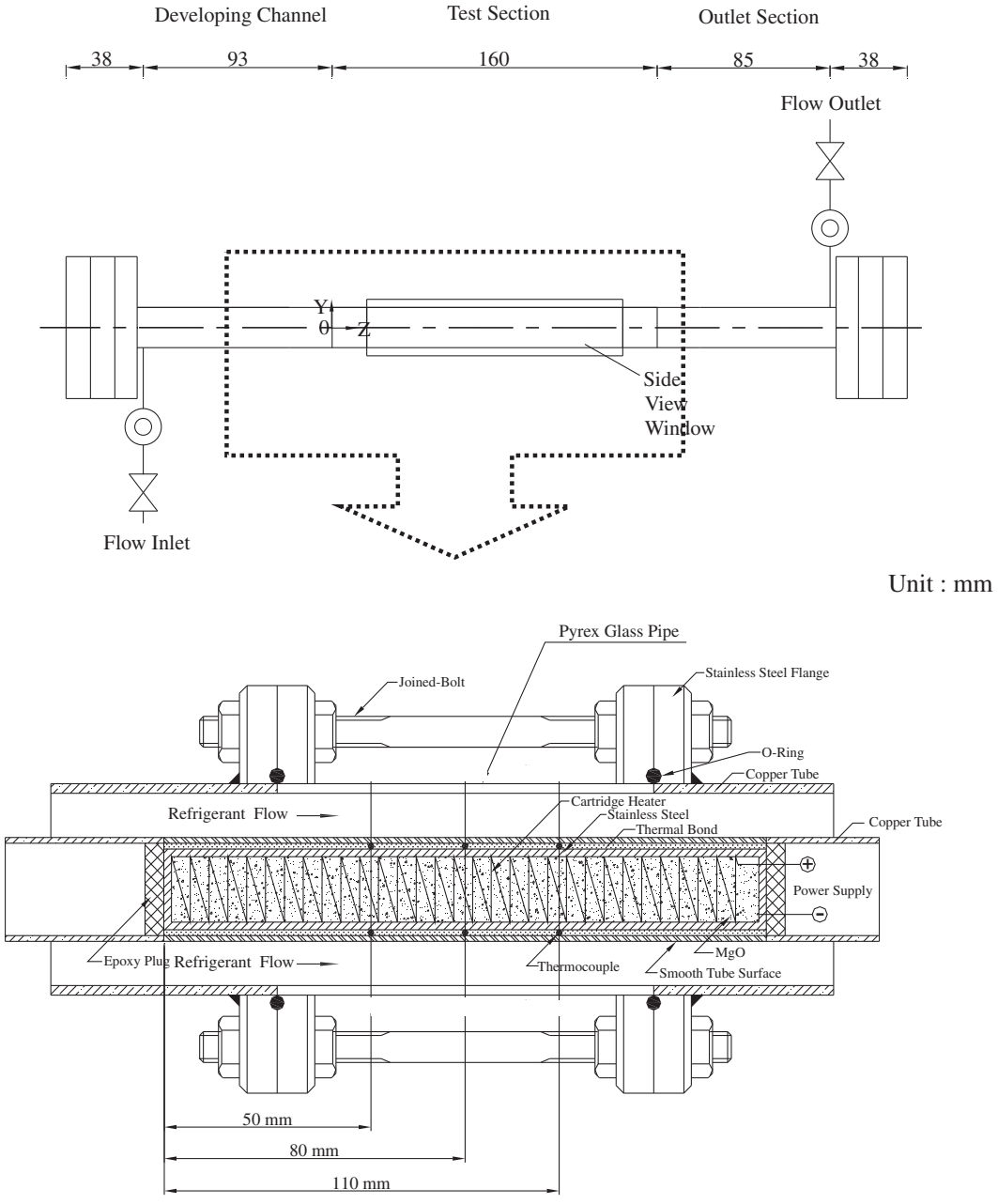

Fig. 2. The detailed arrangement of the test section for the annular duct.

R-134a and R-407C and with some existing correlations are made. Finally, empirical equations to correlate the present data are proposed.

It is of interest to point out that for all cases examined here the maximum vapor quality at $z = 80$ mm is below 0.06 which is estimated by the overall energy balance [45]. At the test section inlet R-410A is at saturated liquid state ($x = 0$).

4.1. Saturated flow boiling curves

The effects of the experimental parameters including the R-410A mass flux and saturated temperature and the gap size of the duct on the boiling curves measured at the middle axial location ($z = 80$ mm) of the narrow annular duct are illustrated in Fig. 3. The results in Fig. 3 indicate that at a low imposed heat flux the wall superheat of the heating surface is lower than that required for the onset of nucleate boiling (ONB) and no bubble nucleates from the heating surface. The flow is in single-phase state. As the imposed wall heat flux is raised gradually, the wall superheat increases correspondingly. At a certain wall superheat bubbles start to nucleate from the heating surface and we have ONB in the flow. Beyond the ONB there is a significant increase in the slope of the boiling curves, implying that a small rise in the wall superheat causes a large increase in the heat transfer rate from the wall to refrigerant. Note that at increasing refrigerant mass flux the boiling curve shifts slightly to the left when the imposed heat flux increases (Fig. 3(a)), which indicates that at a higher refrigerant mass flux the heat transfer in the saturated flow boiling is slightly better. This suggests that at a sufficiently high mass flux the flow boiling can change from the nucleation dominance to convection dominance due to the diminishing bubble nucleation in the heated surface at increasing refrigerant mass flux. The results in Fig. 3(a) also indicate that the required imposed heat flux and wall superheat to achieve ONB are influenced noticeably

Table 1
Summary of the uncertainty analysis.

Parameter	Uncertainty
Annular pipe geometry	
Length, width and thickness (%)	±1.0%
Area (%)	±2.0%
Parameter measurement	
Temperature, T (°C)	±0.2
Temperature difference, ΔT (°C)	±0.3
System pressure, P (kPa)	±2
Mass flux of refrigerant, G (%)	±2
Saturated flow boiling heat transfer	
Imposed heat flux, q (%)	±4.5
Heat transfer coefficient, h_r (%)	±14.5

by the mass flux. Specifically, the required imposed heat flux and wall superheat to achieve ONB are slightly higher for a higher mass flux due to the thinner thermal boundary layer. Then, the data shown in Fig. 3(b) indicate that the boiling curve shifts slightly to the right for a reduction in the refrigerant saturated temperature. Besides, the wall superheat at ONB is not noticeably affected by T_{sat}. Finally, the effects of the duct size on the boiling curves are shown in Fig. 3(c). It is noted that the boiling curve shifts significantly to the left as the duct gap is reduced, indicating that the boiling heat transfer in the smaller duct is substantially better. It is also evident from the data that a lower wall superheat is needed to initiate boiling on the heated surface for the smaller duct. This mainly results from the fact that for given G, q and T_{sat} the liquid Reynolds number of the flow in the duct is lower for a smaller gap. Thus the thermal boundary layer over the heating surface is thicker for a small gap.

4.2. Saturated flow boiling heat transfer coefficients

The saturated flow boiling heat transfer coefficients of R-410A measured at the middle axial location in the narrow annular duct affected by the three experimental parameters are shown in Fig. 4. The results indicate that at given G, δ and T_{sat} the R-410A saturated boiling heat transfer coefficient increases substantially with the imposed heat flux. For example, at T_{sat} = 15 °C, δ = 1.0 mm and G = 500 kg/m^2 s, the saturated boiling heat transfer coefficient for q = 45 kW/m^2 is about 140% higher than that for q = 7 kW/m^2 (Fig. 4(a)). This large increase in h_r is ascribed to the higher active nucleation site density on the heating surface, higher bubble departure frequency and faster bubble growth for a higher imposed heat flux. And the flow boiling heat transfer coefficient increases noticeably with increasing refrigerant mass flux and saturated temperature and with decreasing gap size of the duct at high imposed heat fluxes. For example, at T_{sat} = 15 °C, δ = 1.0 mm and q = 45 kW/m^2, the saturated boiling heat transfer coefficient for G = 700 kg/m^2 s is about 14% higher than that for G = 400 kg/m^2 s (Fig. 4(a)). Besides, at q = 45 kW/m^2, δ = 1.0 mm and G = 500 kg/m^2 s, the saturated boiling heat transfer coefficient for T_{sat} = 15 °C is about 6% higher than that for T_{sat} = 10 °C (Fig. 4(b)). Finally, at q = 45 kW/m^2, T_{sat} = 15 °C and G = 400 kg/m^2 s the saturated boiling heat transfer coefficient for δ = 1.0 mm is about 32% higher than that for δ = 2.0 mm (Fig. 4(c)). This much higher h_r in the smaller duct results from the fact that the shear stress of the flow acting on the heated surface in a smaller channel becomes higher and hence the nucleation bubbles on the heating surface can more easily depart from the heated surface. Moreover, the flow pattern changes from a bubbly flow to a slug flow at lower imposed heat flux for δ = 1.0 mm due to the more severe confinement of the duct walls on the boiling flow. These effects are thought to be the main reasons for the enhancement of nucleate and convection boiling heat transfer when the channel size is reduced.

4.3. Bubble characteristics in saturated flow boiling

The photos of the R-410A boiling flow for the cases at different refrigerant mass fluxes, duct sizes, saturated temperatures and imposed heat fluxes taken from a small region around the middle axial location are shown in Fig. 5. First of all, it is noted from the photo taken from the duct for δ = 1.0 mm shown in Fig. 5(a) for

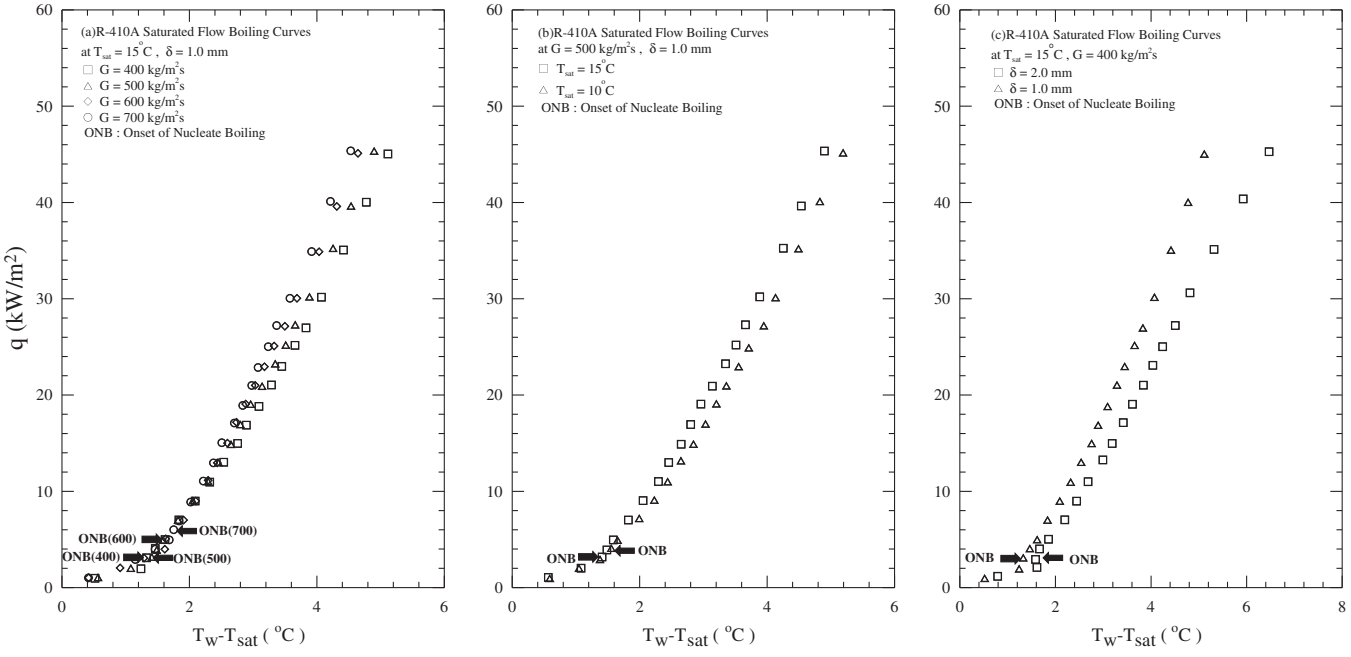

Fig. 3. Saturated flow boiling curves of R-410A: (a) for various refrigerant mass fluxes at T_{sat} = 15 °C and δ = 1 mm, (b) for various saturated temperatures at G = 500 kg/m^2 s and δ = 1 mm, and (c) for various gap sizes at T_{sat} = 15 °C and G = 400 kg/m^2 s.

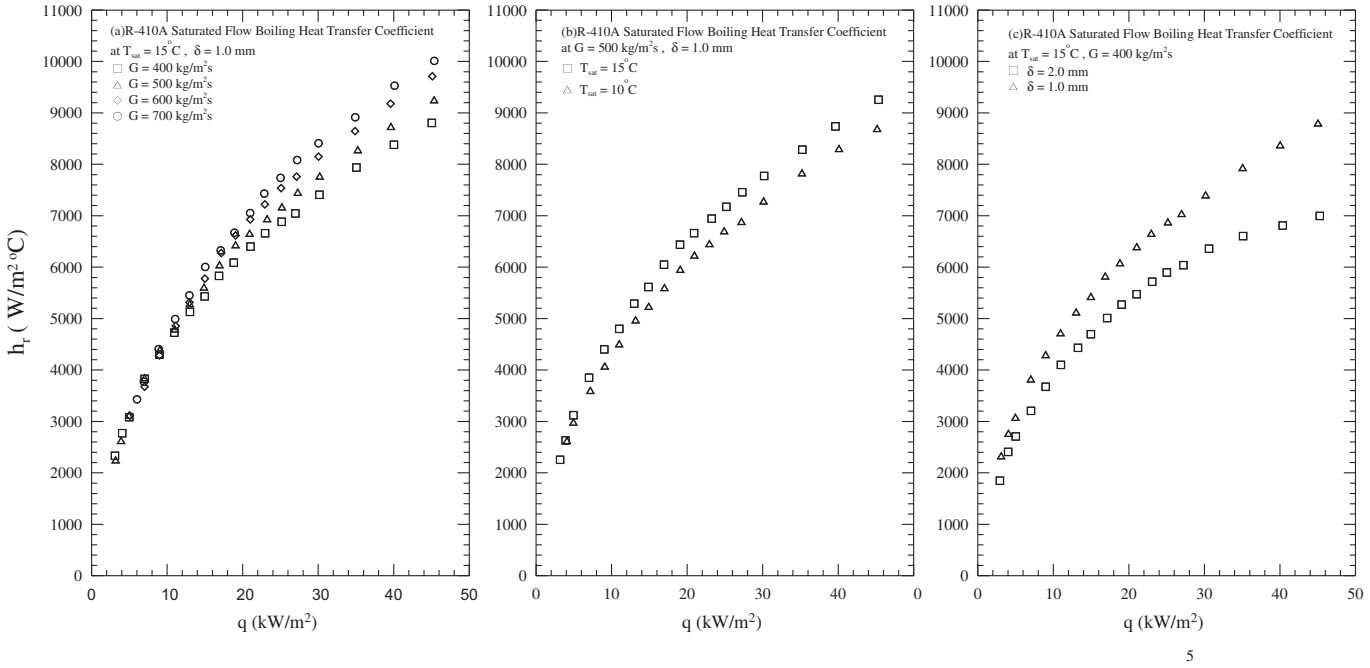

Fig. 4. Saturated flow boiling heat transfer coefficients of R-410A: (a) for various refrigerant mass fluxes at T_{sat} = 15 °C and δ = 1 mm, (b) for various saturated temperatures at G = 500 kg/m^2 s and δ = 1 mm, and (c) for various gap sizes at T_{sat} = 15 °C and G = 400 kg/m^2 s.

the case at T_{sat} = 15 °C and G = 500 kg/m^2 s at the imposed heat flux q = 15 kW/m^2 that a lot of discrete bubbles nucleate from and slide along the heating surface, implying that many bubble nucleation sites are activated. As the imposed heat flux is increased to q = 25 kW/m^2, the active bubble nucleation site density increases and some coalescence bubbles appear (Fig. 5(b)). More coalescence bubbles are seen and they are confined by the duct wall as the heat flux is raised to q = 35 kW/m^2 (Fig. 5(c)). The results in Fig. 5(a)–(f) indicate that at a higher mass flux the liquid refrigerant moves at a higher speed, which in turn tends to sweep the bubbles more quickly away from the heating surface. Besides, the bubble departure frequency is higher and the bubbles are smaller and in violent agitating motion. However, the higher liquid speed causes the shorter time that the refrigerant can be heated. Thus more energy is needed to activate the nucleation sites on the heated surface, resulting in a smaller active nucleation site density at a higher mass flux. Note that at the low mass flux and high imposed heat flux bubble coalescence is more important and a number of bigger bubbles form in the duct. Then, the effects of the refrigerant saturation temperature on the bubble characteristics are illustrated by comparing the photos in Fig. 5(a)–(c) with Fig. 5(g)–(i). The results indicate that at a lower refrigerant saturation temperature the

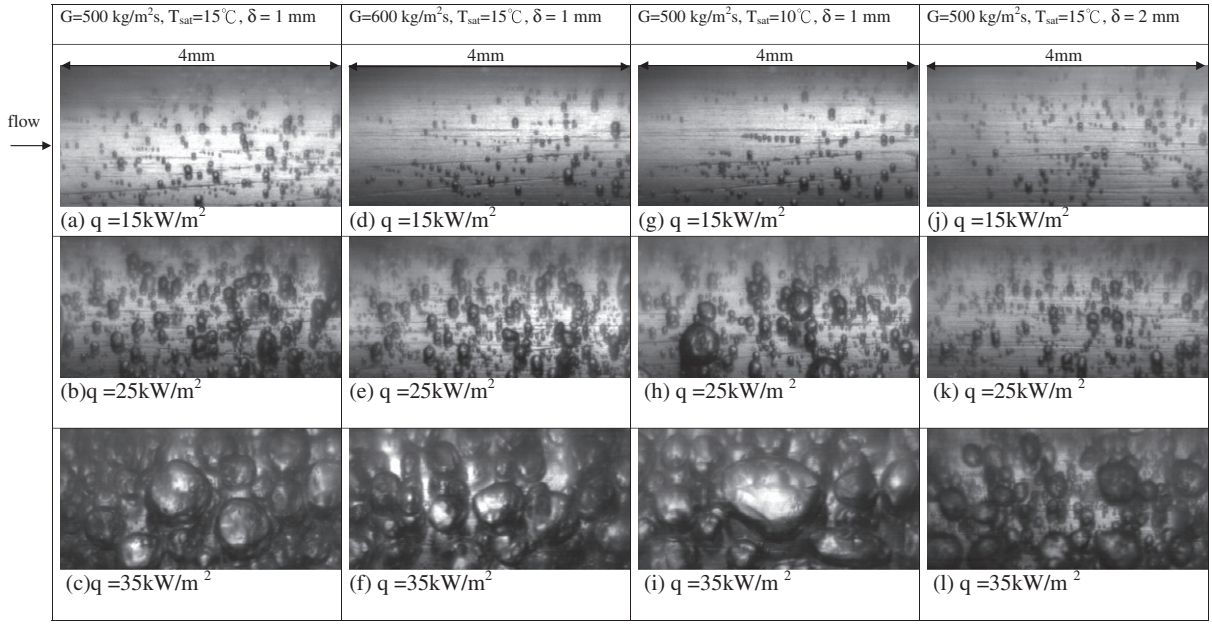

Fig. 5. Photos of bubbles in the saturated flow boiling of R-410A in a small region around middle axial location for various imposed heat flux, mass fluxes, saturated temperature and gap sizes.

bubbles grow bigger before departing from the heated surface due to the higher surface tension force. Besides, at a lower T_{sat} the active nucleation site density is lower due to the higher surface tension and enthalpy of vaporization. Finally, the effects of the duct size on the bubble characteristics are shown by comparing the photos in Fig. 5(a)-(c) with Fig. 5(j)–(l). It is noted that slightly more bubbles and active bubble nucleation sites appear in the smaller duct size at the same imposed heat flux $q = 15$ kW/m^2 (Fig. 5(a) and (j)). As the imposed heat flux is increased to $q = 25$ kW/m^2 (Fig. 5(b) and (k)), the bubble departure frequency is higher and the bubbles collide and coalesce more frequently in the smaller duct due to the higher shear force at reducing duct gap. As the heat flux is raised further to $q = 35$ kW/m^2 (Figs. 5(c) and (l)), the bubbles in the smaller duct coalesce more easily and form bigger bubbles due to the more significant confinement of the duct walls. At even higher imposed heat flux, the flow pattern in the middle portion of the small duct with $\delta = 1.0$ mm changes from a bubbly flow regime to a slug flow regime.

To be quantitative on the bubble characteristics, we estimate the average bubble departure diameter and frequency and the number density of the active nucleation sites on the heating surface from the images of the boiling flow stored in the video tapes. The results from this estimation are examined in the following. The effects of the experimental parameters on the mean bubble departure diameter for the saturated flow boiling of R-410A at the middle axial location in the annular duct are shown in Fig. 6. First, the effects of the refrigerant mass flux shown in Fig. 6(a) indicate that the average departing bubble is only slightly larger for a lower refrigerant mass flux. Then, the results in Fig. 6(b) indicate that the average bubble departure diameter is somewhat smaller for a higher refrigerant saturated temperature. Finally, it is of interest to note from the data given in Fig. 6(c) that the effects of the duct gap on the bubble departure diameter are relatively small. Note that the departing bubble is larger at a higher imposed heat flux. It is worth mentioning that even the size of the largest departing bubble is below 0.08 mm which is much smaller than the diameter of the outer glass pipe in the test section ($D_p = 20.0$ mm). Thus the observation of the bubble size through the curved surface of the glass pipe is not expected to produce significant error.

How the bubble departure frequency is affected by the three parameters for the saturated flow boiling of R-410A at the middle axial location in the annular duct is shown in Fig. 7. Note that the increase of the bubble departure frequency with the imposed heat flux is rather significant for all cases presented here. Besides, the bubble departure frequency is higher at higher refrigerant mass flux and saturated temperature and smaller duct size.

The associated number density of the active nucleation sites affected by the experimental parameters is manifested in Fig. 8. The data clearly show the substantial increase of the active nucleation site density with the imposed heat flux for all cases examined here. It is noted that the active nucleation site density is higher with lower refrigerant mass flux and higher refrigerant saturated temperature especially at high imposed heat flux. The data shown in Fig. 8(c) indicate that the effect of the duct gap on the average active nucleation site density is insignificant.

4.4. Comparison with data for R-134a and R-407C flow boiling

We move further to compare the present data for the R-410A saturated flow boiling with the measured data for R-134a and R-407C flow boiling from Lie et al. [38] and Hsieh et al. [40] in the same narrow annular duct. The comparison is illustrated in Fig. 9. The boiling curves for various refrigerants shown in Fig. 9(a) indicate that much higher imposed heat fluxes are needed to initiate nucleate boiling for R-134a and R-407C. This can be attributed to the lower surface tension for R-410A. Besides, the slope of the boiling curve for R-410A is much steeper, suggesting the saturated flow boiling heat transfer for R-410A is much better. Indeed, the data in Fig. 9(b) manifest that R-410A has a much higher boiling heat transfer coefficient especially at a high imposed heat flux.

Moreover, Fig. 10 illustrates how the bubble characteristics are affected by the three refrigerants. The data clearly show that at the same G, T_{sat} and δ refrigerant R-410A has a much smaller

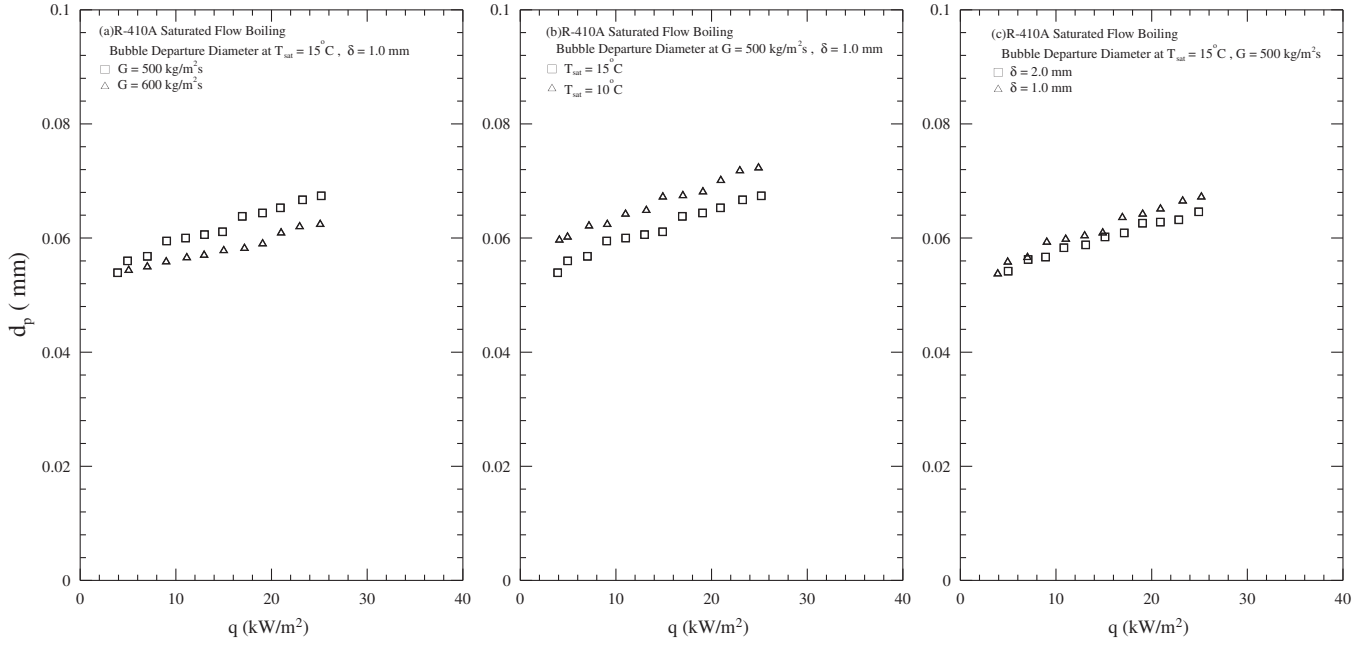

Fig. 6. Mean bubble departure diameter for saturated flow boiling of R-410A: (a) for various refrigerant mass fluxes at $T_{sat} = 15$ °C and $\delta = 1$ mm, (b) for various saturated temperatures at $G = 500$ kg/m^2 s and $\delta = 1$ mm, and (c) for various gap sizes at $T_{sat} = 15$ °C and $G = 500$ kg/m^2 s.

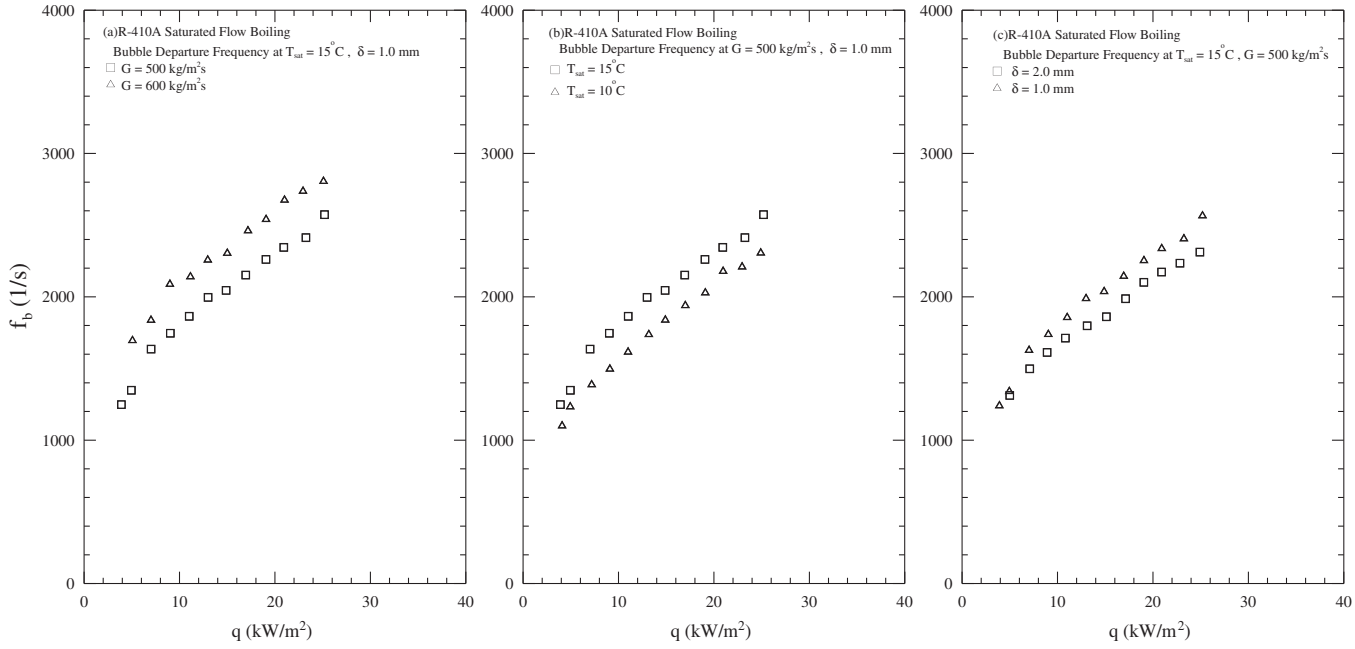

Fig. 7. Mean bubble departure frequency for saturated flow boiling of R-410A: (a) for various refrigerant mass fluxes at T_{sat} = 15 °C and δ = 1 mm, (b) for various saturated temperatures at G = 500 kg/m^2 s and δ = 1 mm, and (c) for various gap sizes at T_{sat} = 15 °C and G = 500 kg/m^2 s.

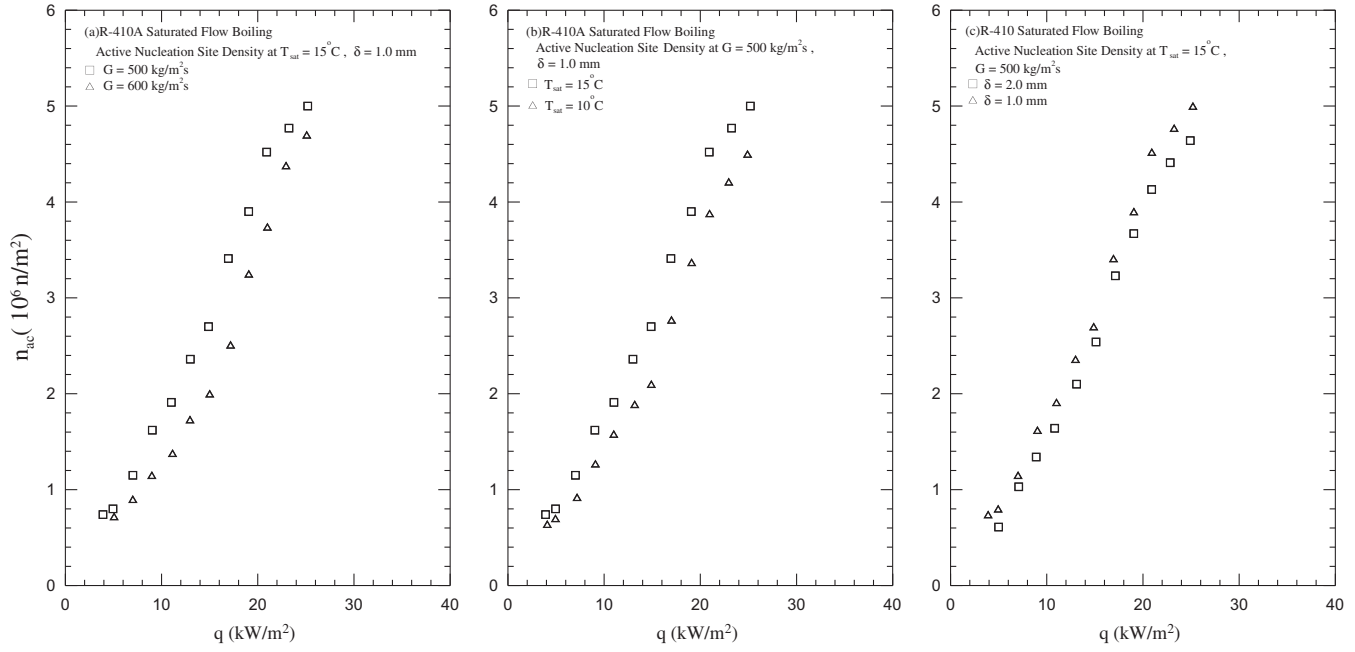

Fig. 8. Mean active nucleation site density for saturated flow boiling of R-410A: (a) for various refrigerant mass fluxes at T_{sat} = 15 °C and δ = 1 mm, (b) for various saturated temperatures at G = 500 kg/m^2 s and δ = 1 mm, and (c) for various gap sizes at T_{sat} = 15 °C and G = 500 kg/m^2 s.

bubble departure size but much higher bubble departure frequency and active nucleation site density especially at high heat fluxes. This again can be attributed mainly to a much lower surface tension of R-410A.

4.5. Comparison with some existing correlations

Furthermore, the present data for the R-410A saturated flow boiling heat transfer coefficient are compared with some existing empirical correlations proposed in the open literature. The results from this comparison are shown in Fig. 11. Note that the correlation from Lazarek and Black [33] overpredicts our data (Fig. 11(a)). Similarly, the correlation from Fujita et al. [34] underpredict our data to a large degree (Fig. 11(b)). However, our data are well correlated by the correlations of Tran et al. [5], Bao et al. [4], Liu and Winterton [31], and Kandlikar [35].

4.6. Correlation equations

According to boiling mechanisms [28], the heat transfer in the bubbly flow regime in the flow boiling can be roughly considered as a combination of single-phase liquid forced convection heat

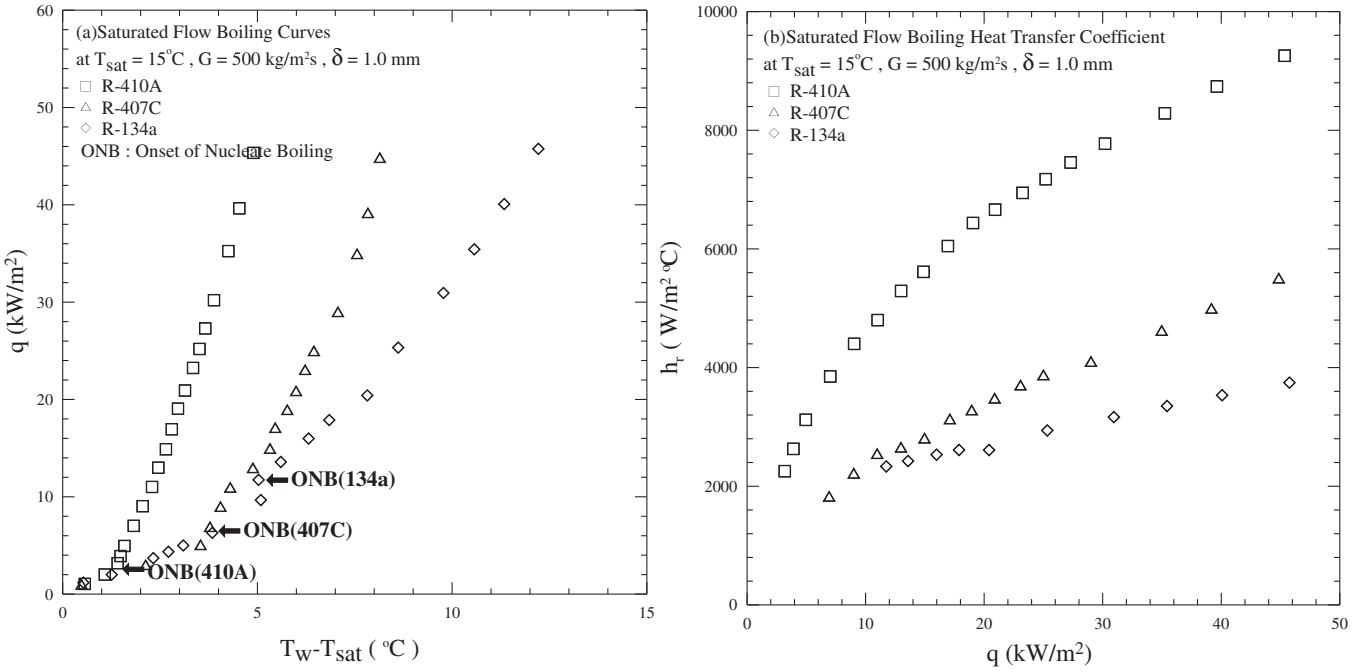

Fig. 9. Comparison of R-410A, R-407C and R-134a saturated flow boiling for (a) boiling curves and (b) boiling heat transfer coefficient.

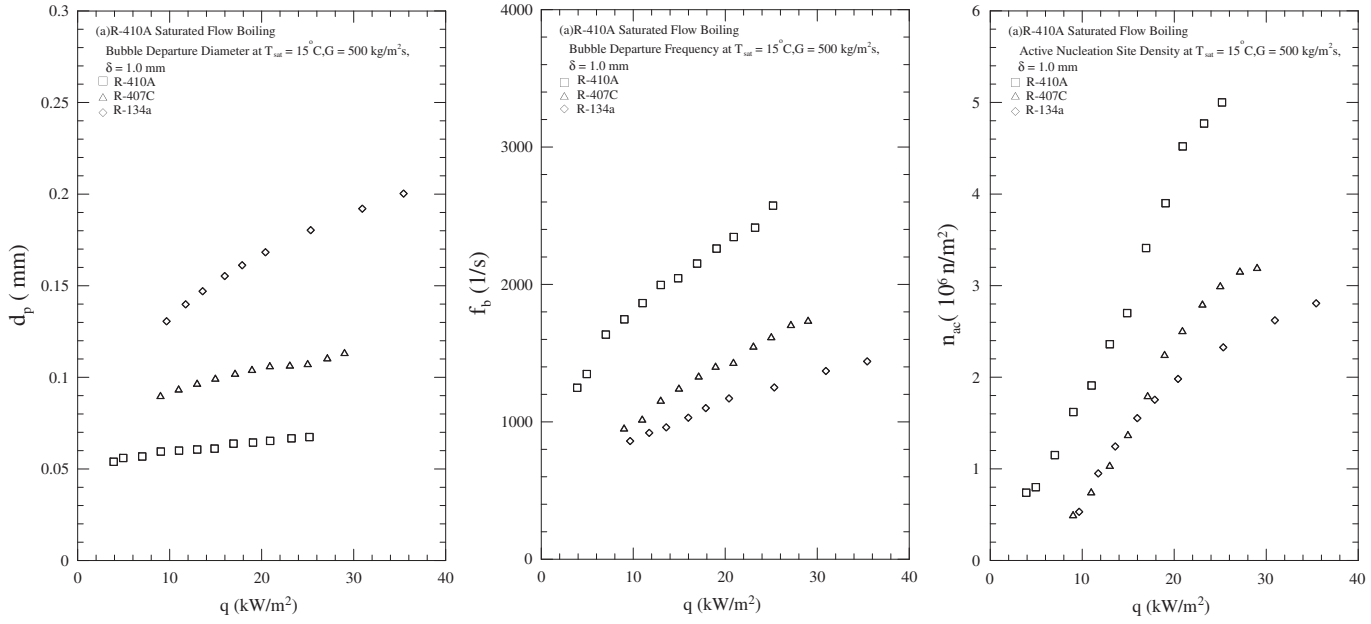

Fig. 10. Comparison of bubble characteristics in R-410A, R-407C and R-134a saturated flow boiling for (a) mean bubble departure diameter, (b) mean bubble departure frequency, and (c) mean active nucleation site density.

transfer q_c and pool boiling heat transfer q_b. Thus the total heat flux input to the boiling flow q_t can be expressed as

$$q_t = q_b + q_c \tag{2}$$

Here q_b and q_c can be respectively calculated from the relations

$$q_b = \rho_g V_g f n_{ac} i_{fg} \tag{3}$$

and

$$q_c = E h_l \Delta T_{sat} \tag{4}$$

Note that in the above equation, an enhancement factor E is added to q_c to account for the agitating motion of the bubbles which can enhance the single-phase convection heat transfer. Empirically, E and h_l can be correlated as

$$E = N_{conf}^{0.01} \mathrm{Fr}_l^{0.1} (1 + 100\mathrm{Bo})^5 \tag{5}$$

and

$$h_l = \mathrm{Nu}_l k_l / \mathrm{D_h} \tag{6}$$

and Nu_l is estimated from the Gnielinski correlation [44],

$$\mathrm{Nu}_l = \frac{(f_f/8)(\mathrm{Re}_l - 1000)\mathrm{Pr}_l}{1 + 12.7\sqrt{f_f/8}(\mathrm{Pr}^{2/3} - 1)} \quad \text{for } \mathrm{Re}_l \geqslant 2300 \tag{7}$$

Here the friction factor f_f is evaluated from the relation

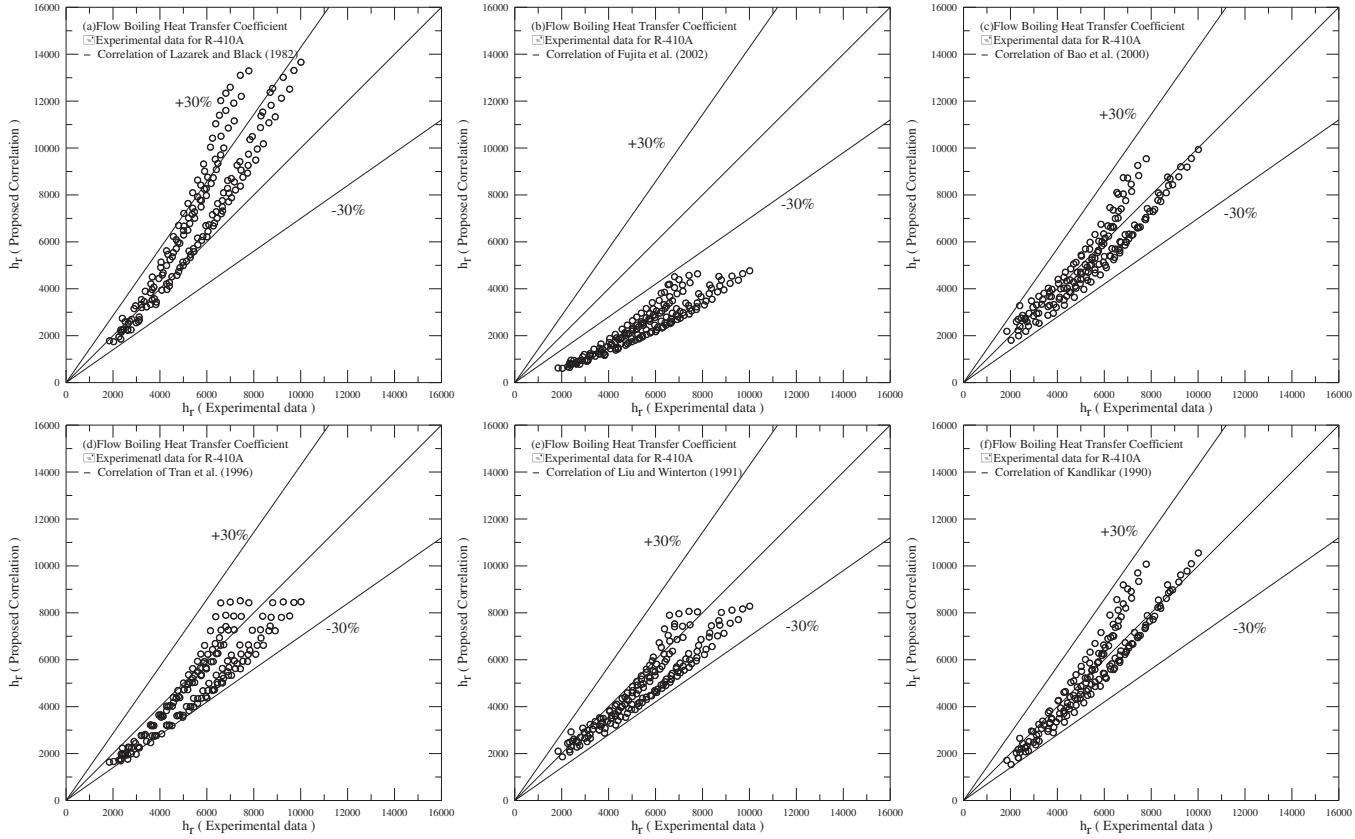

Fig. 11. Comparison of the present data for heat transfer coefficient in the saturated flow boiling of R-410A with existing correlations.

$$f_f = (1.82 \times \log_{10}\mathrm{Re}_l - 1.64)^{-2} \tag{8}$$

Moreover, the Reynolds number of the liquid flow is defined as

$$\mathrm{Re}_l = GD_h(1-x)/\mu_l \tag{9}$$

In Eq. (3), V_g is the mean vapor volume of a departing bubble which is equal to $\frac{4\pi}{3}\left(\frac{d_p}{2}\right)^3$.

Because the range of the experimental Re_l is between 5600 to 11,500, we use the Gnielinski correlation for $\mathrm{Re}_l > 2300$ to estimate the single-phase convection heat transfer. It is difficult to distinguish the individual bubbles at a higher imposed heat flux since many big bubbles form due to the prominent effects of the bubble merging, which in turn overshadows the small bubbles departing from the heating surface. Hence the above correlations do not apply to the data for $q > 25$ kW/m^2.

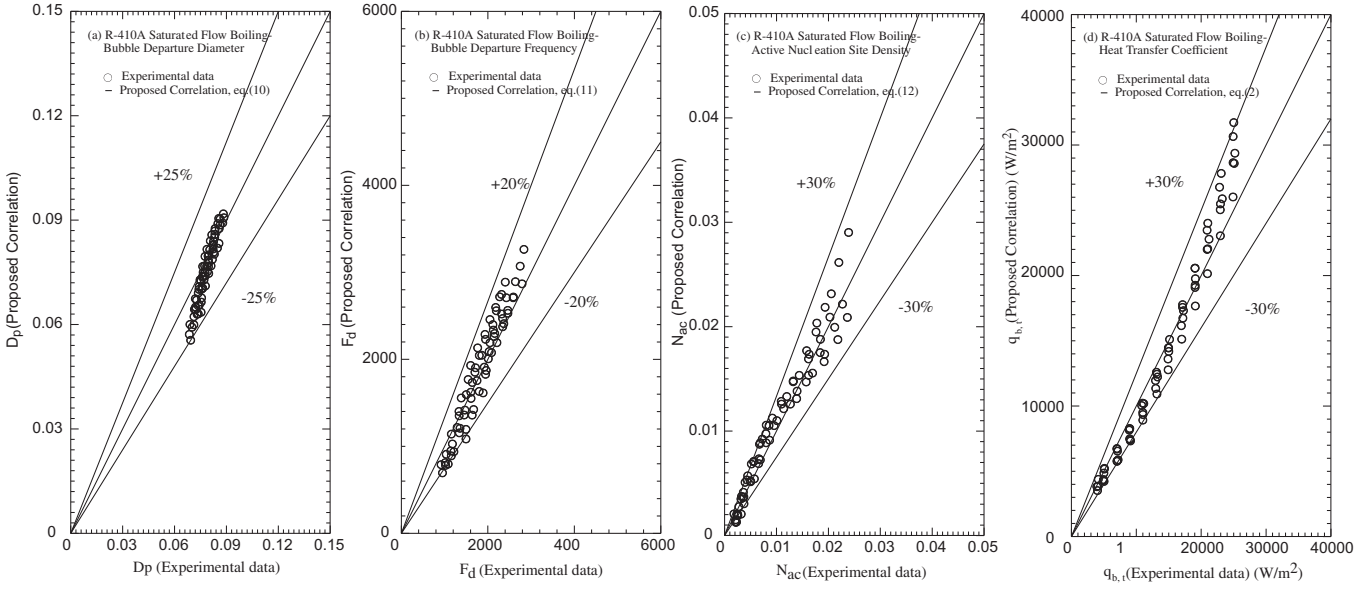

Fig. 12. Comparison of the measured data for mean bubble departure diameter (a), mean bubble departure frequency (b), mean active nucleation site density (c), and heat transfer coefficient (d) in the saturated flow boiling of R-410A with the proposed correlations.

To enable the usage of the above correlation for the flow boiling heat transfer, the mean departing bubble diameter and departure frequency and the active nucleation density on the heating surface need to be correlated in advance. The average bubble departure diameter in the saturated flow boiling of R-410A in the narrow annular duct estimated from the present flow visualization can be correlated as

$$D_p = \frac{d_p}{\sqrt{\sigma/(g\Delta\rho)}} = 0.7\left(\frac{\rho_l}{\rho_g}\right)^{0.5} \mathrm{Re}_l^{-0.25} \cdot \mathrm{Bo}^{0.2} \cdot N_{\mathrm{conf}}^{-0.2} \quad (10)$$

Fig. 12(a) shows that almost all the present experimental data for d_p fall within ±20% of the above correlation and the mean absolute error is 5.8%. Besides, an empirical equation is proposed for the product of the mean bubble departure diameter and departure frequency as

$$F_d = \frac{f \cdot d_p}{\mu_l(\rho_l D_h)} = 2.2\mathrm{Re}_l^{1.4} \cdot \mathrm{Pr}_l^2 \cdot \mathrm{Bo}^{0.7} \cdot N_{\mathrm{conf}} \quad (11)$$

Note that almost all the experimental data collected in this study can be correlated within ±20% by Eq. (11) and the mean absolute error is 10.9% (Fig. 12(b)). Finally, we propose an empirical correlation for the average active nucleation site density in the saturated flow boiling of R-410A in the narrow annular duct as

$$N_{\mathrm{AC}} = n_{\mathrm{ac}} d_p^2 = -0.001 + 500\mathrm{Bo}^{1.25}\mathrm{Re}_l^{0.05} N_{\mathrm{conf}}^{0.06} \quad (12)$$

Fig. 12(c) shows that the present experimental data fall within ±25% of the above correlation and the mean absolute error is 14.8%.

When the correlations for d_p, f, and n_{ac} given in Eqs. (10)–(12) are combined with Eqs. (2)–(9) for q_t, most boiling heat transfer data measured in the present study fall within ±20% of the correlation proposed here with the mean deviation of 9.3% (Fig. 12(d)). Note that the data for $q > 20$ kW/m^2 are overpredicted by the above correlations.

5. Concluding remarks

The experimental heat transfer data for the saturated flow boiling of R-410A in the narrow annular duct have been presented here. Meanwhile, the bubble behavior in the boiling flow is examined. The effects of the imposed heat flux, refrigerant mass flux, saturated temperature, and duct size on the R-410A saturated flow boiling heat transfer coefficient and associated bubble characteristics have been investigated in detail. Moreover, comparisons of the present data with that for R-134a and R-407C and with some existing correlations are conducted. The major results obtained here can be summarized in the following:

(1) The boiling heat transfer coefficients increase with increasing refrigerant mass flux and saturated temperature and with a decrease in the gap size. Besides, raising the imposed heat flux can cause a significant increase in the boiling heat transfer coefficient.

(2) The results from the flow visualization show that the mean diameter of the bubbles departing from the heating surface decreases slightly with increasing refrigerant mass flux and saturated temperature. Besides, at a high imposed heat flux many bubbles generated from the cavities in the heating surface tend to merge together to form big bubbles. The bubble departure frequency increases at increasing refrigerant mass flux and saturated temperature and at decreasing duct size. The active nucleation site density is much lower at a higher refrigerant mass flux and a lower saturation temperature.

(3) The boiling heat transfer coefficient, mean bubble departure diameter, bubble departure frequency and active nucleation site density in the R-410A saturated flow boiling are correlated in terms of the relevant dimensionless groups.

Acknowledgments

The financial support of this study by the engineering division of National Science Council of Taiwan, ROC through the contract NSC 96-2221-E-009-133-MY3 is greatly appreciated.

References

[1] S.M. Ghiaasiaan, Two-Phase Flow Boiling, and Condensation in Conventional and Miniature Systems, Cambridge, 2008.
[2] S.G. Kandlikar, W.J. Grande, Evolution of microchannel flow passages-thermohydraulic performance and fabrication technology, Heat Transfer Eng. 24 (1) (2003) 3–17.
[3] P.A. Kew, K. Cornwell, Correlations for the prediction of boiling heat transfer in small-diameter channels, Appl. Therm. Eng. 17 (1997) 705–715.
[4] Z.Y. Bao, D.F. Fletcher, B.S. Haynes, Flow boiling heat transfer of Freon R11 and HCFC123 in narrow passages, Int. J. Heat Mass Transfer 43 (18) (2000) 3347–3358.
[5] T.N. Tran, M.W. Wambsganss, D.M. France, Small circular- and rectangular-channel boiling with two refrigerants, Int. J. Multiphase Flow 22 (1996) 485–498.
[6] B. Agostini, A. Bontemps, Vertical flow boiling of refrigerant R134a in small channels, Int. J. Heat Fluid Flow 26 (2005) 296–306.
[7] S.G. Kandlikar, M.E. Steinke, Flow boiling heat transfer coefficient in minichannels – correlation and trends, in: Proceedings of the Twelfth International Heat Transfer Conference, vol. 3, 2002, pp. 785–790.
[8] S. Lin, P.A. Kew, K. Cornwell, Two-phase heat transfer to a refrigerant in a 1mm diameter tube, Int. J. Refrig. 24 (1) (2001) 51–56.
[9] B. Watel, Review of saturated flow boiling in small passages of compact heat exchangers, Int. J. Therm. Sci. 42 (2003) 107–140.
[10] C.C. Wang, J.G. Yu, P.L. Shieh, D.C. Lu, An experimental study of convective boiling of refrigerants R-22 and R-410A, ASHRAE Trans. 121 (1998) 1144–1150.
[11] T. Ebisu, K. Torikoshi, Heat transfer characteristics and correlations for R-410A flowing inside a horizontal smooth tube, ASHRAE Trans. 121 (1998) 556–561.
[12] Y.Y. Hsieh, Y.M. Lie, T.F. Lin, Saturated flow boiling heat transfer of refrigerant R-410A in a horizontal annular finned duct, Int. J. Heat Mass Transfer 50 (2007) 1442–1454.
[13] Y.Y. Hsieh, T.F. Lin, Saturated flow boiling heat transfer and pressure drop of refrigerant R-410A in a vertical plate heat exchanger, Int. J. Heat Mass Transfer 45 (2002) 1033–1044.
[14] Y.Y. Hsieh, T.F. Lin, Evaporation heat transfer and pressure drop of refrigerant R-410A flow in a vertical plate heat exchanger, ASME J. Heat Transfer 125 (2003) 852–857.
[15] G.A. Longo, A. Gasparella, HFC-410A vaporization inside a commercial brazed plate heat exchanger, Exp. Therm. Fluid Sci. 32 (2007) 107–116.
[16] I.K. Kim, J.H. Park, Y.H. Kwon, Y.S. Kim, Experimental study on R-410a evaporation heat transfer characteristics in oblong shell and plate heat exchanger, Heat Transfer Eng. 28 (7) (2007) 633–639.
[17] L.M. Schlager, M.B. Pate, A.E. Bergles, Performance predictions of refrigerant-oil mixtures in smooth and internally finned tubes-Part I: literature review, ASHRAE Trans. 96 (1) (1999) 160–169.
[18] L.M. Schlager, M.B. Pate, A.E. Bergles, Performance predictions of refrigerant-oil mixtures in smooth and internally finned tubes – Part II: design equation, ASHRAE Trans. 96 (1) (1999) 170–182.
[19] A. Gidwani, M.M. Ohadi, M. Salehi, In-tube condensation of refrigerant and refrigerant-oil mixtures – a review of most recent work, ASHRAE Trans. 104 (1B) (1998) 1322–1332.
[20] O. Lottin, P. Guillemet, J.M. Lebreton, Effects of synthetic oil in a compression refrigeration system using R410A. Part I: modeling of the whole system and analysis of its response to an increase in the amount of circulation oil, Int. J. Refrig. 26 (2003) 772–782.
[21] K. Cornwell, P.A. Kew, Boiling in small parallel channels, in: P.A. Pilavachi (Ed.), Energy Efficiency in Process Technology, Elsevier Applied Science, London, 1993, pp. 624–638.
[22] C.P. Yin, Y.Y. Yan, T.F. Lin, B.C. Yang, Subcooled flow boiling heat transfer of R-134a and bubble characteristics in a horizontal annular duct, Int. J. Heat Mass Transfer 43 (2000) 1885–1896.
[23] R. Situ, Y. Mi, M. Ishii, M. Mori, Photographic study of bubble behaviors in forced convection subcooled boiling, Int. J. Heat Mass Transfer 47 (2004) 3659–3667.
[24] R. Maurus, V. Ilchenko, T. Sattelmayer, Automated high-speed video analysis of the bubble dynamics in subcooled flow boiling, Int. J. Heat Fluid Flow 25 (2004) 149–158.

[25] S.H. Chang, I.C. Bang, W.P. Baek, A photographic study on the near-wall bubble behavior in subcooled flow boiling, Int. J. Therm. Sci. 41 (2002) 609–618.
[26] V.H. Del Balle, D.B.R. Kenning, Subcooled flow boiling at high heat flux, Int. J. Heat Mass Transfer 28 (10) (1985) 1907–1920.
[27] T. Okawa, T. Ishida, I. Kataoka, M. Mori, An experimental study on bubble rise path after the departure from a nucleation site in vertical upflow boiling, Exp. Therm. Fluid Sci. 29 (2005) 287–294.
[28] J.C. Chen, A correlation for boiling heat transfer to saturated fluids in convective flow, Ind. Eng. Chem. Process Des. Dev. 5 (1966) 322–329.
[29] F.W. Dittus, L.M.K. Boelter, Heat transfer in automobile radiator of the tube type, Publication in Engineering, vol. 2, University of California, Berkley, 1930, p. 250.
[30] K.E. Gungor, R.H.S. Winterton, A general correlation for flow boiling in tubes and annuli, Int. J. Heat Mass Transfer 29 (1986) 351–358.
[31] Z. Liu, R.H.S. Winterton, A general correlation for saturated and subcooled flow boiling in tubes and annuli, based on a nucleate pool boiling equation, Int. J. Heat Mass Transfer 34 (1991) 2759–2766.
[32] W. Zhang, T. Hibiki, K. Mishima, Correlation for flow boiling heat transfer in mini-channels, Int. J. Heat Mass Transfer 47 (2004) 5749–5763.
[33] G.M. Lazarek, S.H. Black, Evaporative heat transfer, pressure drop and critical heat flux in a small vertical tube with R-113, Int. J. Heat Mass Transfer 25 (7) (1982) 945–960.
[34] Y. Fujita, Y. Yang, N. Fujita, Flow boiling heat transfer and pressure drop in uniformly heated small tubes, in: Proceedings of the Twelfth International Heat Transfer Conference, vol. 3, 2002, pp. 743–748.
[35] S.G. Kandlikar, A general correlation for two-phase flow boiling heat transfer coefficient inside horizontal and vertical tubes, ASME J. Heat Transfer 102 (1990) 219–228.
[36] S.G. Kandlikar, A model for predicting the two-phase flow boiling heat transfer coefficient in augmented tube and compact heat exchanger geometries, ASME J. Heat Transfer 113 (1991) 966–972.
[37] S.G. Kandlikar, P. Balasubramanian, An extension of the flow boiling correlation to transition, laminar, and deep laminar flows in minichannles and microchannels, Heat Transfer Eng. 25 (2004) 86–93.
[38] Y.M. Lie, T.F. Lin, Saturated flow boiling heat transfer and associated bubble characteristics of R-134a in a narrow annular duct, Int. J. Heat Mass Transfer 48 (25–26) (2005) 5602–5615.
[39] Y.M. Lie, T.F. Lin, Subcooled flow boiling heat transfer and associated bubble characteristics of R-134a in a narrow annular duct, Int. J. Heat Mass Transfer 49 (13-14) (2006) 2077–2089.
[40] F.C. Hsieh, K.W. Li, Y.M. Lie, C.A. Chen, T.F. Lin, Saturated flow boiling heat transfer of R-407C and associated bubble characteristics in a narrow annular duct, Int. J. Heat Mass Transfer 51 (2008) 3763–3775.
[41] C.A. Chen, W.R. Chang, K.W. Li, Y.M. Lie, T.F. Lin, Subcooled flow boiling heat transfer of R-407C and associated bubble characteristics in a narrow annular duct, Int. J. Heat Mass Transfer 52 (2009) 3147–3158.
[42] S.W. Churchill, H.H.S. Chu, Correlating equations for laminar and turbulent free convection from a horizontal cylinder, Int. J. Heat Mass Transfer 18 (1975) 1049–1053.
[43] S.J. Kline, F.A. McClintock, Describing uncertainties in single-sample experiments, ASME Mech. Eng. 75 (1) (1953) 3–12.
[44] V. Gnielinski, New equations for heat and mass transfer in turbulent pipe and channel flow, Int. Chem. Eng. 16 (2) (1976) 359–368.
[45] C.A. Chen, C.Y. Lee, T.F. Lin, Experimental study of evaporation heat transfer of R-134a in a narrow annular duct, Int. J. Heat Mass Transfer 53 (2010) 2218–2228.